Crystallization behaviors and structural study of amorphous $GeCu_2Te_3$

Y. Sutou[1], Y. Saito[1], J. Koike[1], P. Jóvári[2], I. Kaban[3]
[1] Department of Materials Science, Graduate School of Engineering, Tohoku University, 6-6-11 Aoba-yama, Sendai 980-8579, Japan
[2] Wigner Research Center for Physics, Konkoly-Thege str. 29-33., 1121 Budapest, Hungary
[3] IFW Dresden, Institute for Complex Materials, P.O.Box 270116, D-01171 Dresden, Germany
ysutou@material.tohoku.ac.jp (Y. Sutou)

ABSTRACT

The crystallization mechanism of $GeCu_2Te_3$ (GCT) amorphous film prepared by sputter deposition was investigated by differential scanning calorimetry under non-isothermal conditions. From a comparison of the crystallization behaviors of the GCT and GST amorphous films it can be suggested that the GCT amorphous film shows a growth dominated crystallization process. The crystalline GCT film showed lower reflectance than the amorphous GCT film. The nucleation time of the GCT amorphous films was estimated to be 26 ns, while that of the GST amorphous film was about 23 ns. The GCT amorphous structure was investigated by combining experimental techniques of X-ray diffraction and EXAFS.

Key words: crystallization mechanism, nucleation time, reflectance change, amorphous structure.

1. INTRODUCTION

Very recently, the present authors have found that a $GeCu_2Te_3$ (GCT) amorphous film had a high crystallization temperature of over 200˚C and showed higher thermal stability than $Ge_2Sb_2Te_5$ (GST) film [1]. They demonstrated that the GCT memory device showed memory switching behaviors and exhibited a 10% lower power consumption for the reset operation than the conventional GST memory device because of its low melting point of about 500˚C [2]. In addition, the GCT amorphous film was found to show a smaller thickness change, equivalently a small volume change, upon crystallization than the GST, and the changes are of opposite signs for the GCT and GST films [2]. These results indicate that the $GeCu_2Te_3$ compound is a promising phase change material for PCRAM application. However, the crystallization behaviors and the structure of the amorphous GCT film have not been investigated yet. In this study, the crystallization mechanism and nucleation time (crystallization speed) of GCT amorphous films prepared by sputter deposition were investigated by differential scanning calorimetry under non-isothermal conditions and static laser tester, respectively. Moreover, the amorphous structure of GCT investigated by combining experimental techniques such as X-ray diffraction and EXAFS.

2. EXPERIMENTS

GCT films were deposited on SiO_2/Si substrates by RF sputtering of a Ge-Cu-Te alloy target or co-sputtering of GeTe and CuTe targets. $Ge_2Sb_2Te_5$ (GST) films were also prepared by sputtering of a $Ge_2Sb_2Te_5$ alloy target for comparison. Differential scanning calorimetric (DSC) measurements were employed to investigate the crystallization kinetics of the films on the SiO_2/Si substrate at various heating rates of 12 - 50ºC/min in Ar atmosphere. Film thickness for the DSC measurements was set to be 1500 nm in order to clearly detect an exothermic peak for crystallization. The reflectance of the amorphous and crystalline films with a thickness of 200 nm on SiO_2/Si substrates were measured relative to an Al reference mirror with spectrophotometer in the range of wavelength between 300-1000 nm. The nucleation times of the as-deposited GCT and GST amorphous films with a thickness of 200 nm were measured using a static laser tester based on the reflectance results. The wavelength of both the pump and probe laser was 830 nm. Thickness change by laser irradiation was measured by atomic force microscopy (AFM).

The GCT amorphous structure was investigated by combining experimental techniques such as X-ray diffraction (XRD) and extended X-ray absorption fine structure (EXAFS). The GCT amorphous powder with over 50 mg was prepared by RF sputtering of a Ge-Cu-Te alloy target for the measurements. Since a large amount of powder was prepared by long-term sputtering of a Ge-Cu-Te alloy target, the amorphous composition may be deviated from the

stoichiometric value. The energy of the incident radiation for the XRD was 85.0 keV. Ge, Cu and Te EXAFS spectra were measured in transmission mode. The powder sample was mixed with cellulose and pressed into a tablet. The transmission of the tablet was around 1/e at the corresponding edges. Intensities before and after the sample were measured by ionization chambers filled with Ar, Kr and N_2 with partial pressures depending on the edge energy. Structural models were obtained by the Reverse Monte Carlo simulation technique (RMC). Details of the RMC simulation methods for amorphous structural model are described in [3-5]. In the RMC run, experimental datasets are fitted by moving the atoms of a model system (simulation box containing 7500 atoms) randomly until model XRD and EXAFS spectra calculated from the atomic coordinates agree with the experimental data. The density was 6.26 g/cm^3 (0.03882 Å^{-3}) which was estimated from the density of $GeCu_2Te_3$ crystalline phase and the volume change (thickness change) upon crystallization for amorphous GCT.

3. RESULTS & DISCUSSION

3-1. Local activation energy of GCT film

Fig. 1(a) shows the fraction of crystallization x as a function of temperature at different heating rates obtained from the DSC measurements. The temperature interval for crystallization is seen to show less dependence on the heating rates. Based on the results in Fig. 1(a) the local activation energy $E_a(x)$ of crystallization at x is estimated using the following equation proposed by Ozawa for non-isothermal crystallization [6, 7]:

$$\log\beta = \text{const.} - 0.4567E_a(x)/RT \quad (1).$$

Here, β is the heating rate, R is the gas constant and T is the temperature for a given value of x. Fig. 1(b) shows $\log\beta$ plots as a function of $1000/T$ at x = 0.1, 0.3, 0.5, 0.7 and 0.9. The $E_a(x)$ is evaluated from the slopes of the linear fitted lines in Fig. 1(b). Figure 1(c) shows the $E_a(x)$ plots as a function of the x. It is seen that the $E_a(x)$ is almost constant value of 3.0 eV in the range of $x < 0.15$ and then decreases down to about 2.5 eV with increasing x. Meanwhile, it was found that the $E_a(x)$ of the GST film monotonically decreases from about 2.6 eV to about 1.5 eV with increasing x [1]. The variation in $E_a(x)$ as a function of crystallization fraction may be caused by variations in the nucleation and growth processes during crystallization. The overall mean activation energy E_a of the GCT film was 2.78 eV, while that of the GST film was 2.08 eV. These results suggested that the thermal stability of the amorphous GCT film is higher than that of the amorphous GST film.

3-2. Crystallization kinetics

The decrease in the $E_a(x)$ with increasing x, as shown in Fig. 1(c), indicates that the crystallization process is not a single step mechanism but a multi-step process. Lu et al. proposed that a local Avrami exponent $n(x)$ for non-isothermal crystallization can be evaluated from the following equation [8]:

$$n(x) = -R\partial\ln[-\ln(1-x)]/(E_a(x)\,\partial(1/T)) \quad (2).$$

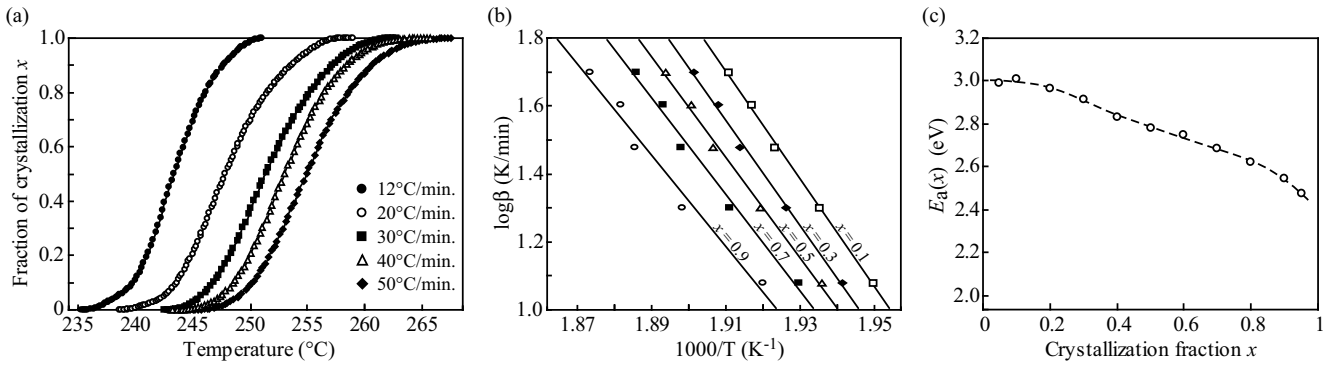

Fig. 1. (a) Crystallization fraction x vs. temperature curves at different heating rates β, (b) Plots of $\log\beta$ vs. $1000/T$ for the crystallization fraction x and (c) Dependence of the activation energy $E_a(x)$ on the crystallization fraction x for the GCT film.

Here, x is the crystallization fraction, R is the gas constant, $E_a(x)$ is the local activation energy and T is the temperature. An Avrami exponent provides information about nucleation and growth mechanisms of crystallization. The local Avrami exponent $n(x)$ of the GCT film was calculated at a heating rate of 30ºC/min by taking account of the variable $E_a(x)$, where the relationship between the $E_a(x)$ and the x was deduced by numerically fitting $E_a(x)$ vs. x curve. Fig. 2 shows the variation in the $n(x)$. The $n(x)$ is found to decrease gradually with increasing x. This result indicates that the crystallization mechanism changes with the progress of crystallization.

It is well known that the Avrami exponent n depends on nucleation and growth mechanisms and is partitioned as follows [9-11]:

$$n = a + bp \qquad (3).$$

Here, a refers to the nucleation rate and is categorized: a=0 for zero nucleation rate; 0<a<1 for decreasing nucleation rate; a=1 for constant nucleation rate; a>1 for increasing nucleation rate. b represents the dimensionality of crystal growth and has the values: b=1 for 1-dimensional growth; b=2 for 2-dimensional growth; b=3 for 3-dimensional growth. p indicates the mechanism that controls crystal growth and has a value of 0.5 for diffusion-controlled growth and has a value of 1 for interface-controlled growth. The GCT film should have p=1 indicating interface-controlled growth because the GCT film polymorphically crystallizes in a $GeCu_2Te_3$ crystalline phase [12]. The result in Fig. 2 supports the following crystallization mechanism of the GCT amorphous film. In the initial range x<0.15 the $n(x)$ is larger than 4, which indicates interface-controlled (p=1) and 3-dimensional (b=3) growth at an increasing nucleation rate (a>1). A higher n of >4 suggests that crystallization involves a transient nucleation process with an increasing nucleation rate [13, 14]. In the range x > 0.15 the $n(x)$ decreases from 4 to about 2. Especially, the $n(x)$ becomes below 2 in the range x>0.8. These results suggest that crystallization of the GCT amorphous film progresses by 3- and 2-dimensional growth at a decreasing nucleation rate and then proceeds by 2- and 1-dimensional growth at zero nucleation rate in the later stage. Meanwhile, although such variation of $n(x)$ was also observed in the GST film, the $n(x)$ of the GST film was higher than that of the GCT film [1]. The $n(x)$ of the GST film was over 4 in the range x<0.5 and decreased from 4 to about 3 in the range x>0.5 [1].

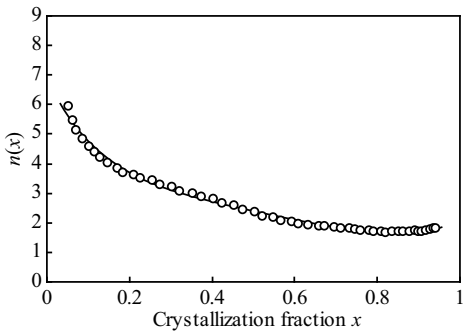

Fig. 2. Local Avrami exponent $n(x)$ vs. crystallization fraction x at β=30 ºC/min.

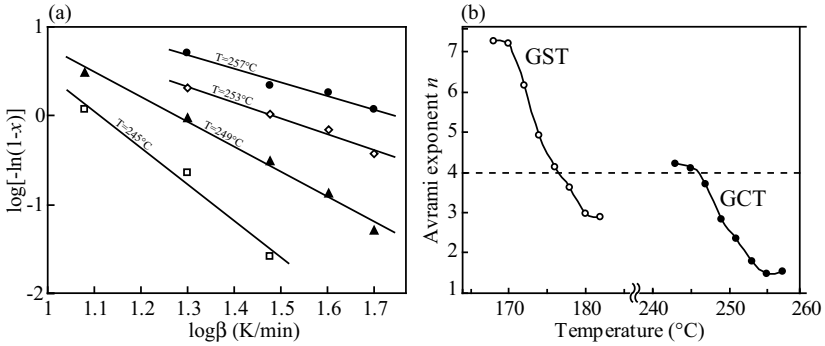

Fig. 3. (a) Plots of log[-ln(1-x)] vs. logβ at different temperature for the GCT film. (b) Temperature dependence of the n for the GCT and GST films..

The temperature dependence on the Avrami exponent n shows more clearly the difference in the crystallization mechanism between the GCT and GST films. Figure 3(a) shows the plots of log[-ln(1-x)] vs. logβ at different temperatures for the GCT film. The slope of each straight line gives the n at temperature T. Figure 3(b) shows the n plots as a function of temperature during crystallization for the GCT and GST films. It is seen that the GST film has a higher n value of over 4, indicating a transient nucleation process with an increasing nucleation rate, except for that in the higher temperature range. This may be due to the fact that the GST film shows a nucleation dominated crystallization process [15, 16]. The n value of the GST films decreases from 4 to about 3 in the higher temperature range, which indicates that the crystallization of the GST film progresses by crystal growth at a decreasing nucleation rate. Nishi et al. have simulated that the temperature of peak nucleation frequency was lower than that of peak crystal growth rate for GST film [16]. The present results for the GST film are good agreement with the simulated results.

Meanwhile, the GCT film shows lower n value below 4, except in the lower temperature range. The lower n value below 4 indicates crystal growth at a decreasing and/or zero nucleation rate. These results suggest that the GCT amorphous film shows a growth dominated crystallization process.

3-3. Nucleation time evaluated by laser beam pulse irradiation

In this section, we show the results of nucleation time of the GCT amorphous film obtained by static laser tester. First, the reflectance of the amorphous and crystalline GCT films is shown. Fig. 4 shows the reflectance of the as-deposited and annealed GCT films, where the annealed sample was heated up to 400°C for complete crystallization. The results of the GST films were also shown for comparison. The GST film annealed up to 400°C possessing crystalline state shows about 20% higher reflectance than the as-deposited GST film with amorphous state in the wavelength range of 300-1000 nm. The difference of the reflectance between the amorphous and crystalline GST films is almost good agreement with the reported results in pseudobinary GeTe-Sb_2Te_3 films [17]. Meanwhile, it is noteworthy that the GCT film shows the opposite change in reflectance with crystallization. The GCT amorphous film has a similar reflectance as the GST amorphous film, but the annealed GCT film possessing crystalline state shows about 10% lower reflectance than the as-deposited amorphous GCT film, in the wavelength range of 300-1000nm. Such a decrease in reflectance upon crystallization has also been recently observed in Fe-Te films [18]. In this study, the nucleation time of the GCT amorphous film was evaluated using the fact that the reflectance decreases with crystallization, although it is not clear at the moment why the reflectance decreases with crystallization for the GCT film.

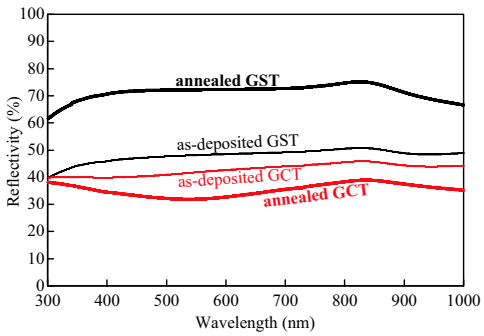

Fig. 4. Reflectance of the as-deposited and annealed GCT films.

Fig. 5 shows the reflectance change induced by laser at power of 11.0 mW and wavelength of 830 nm as a function of a pulse duration (0-80 ns) for the GCT amorphous film. Since the reflectivity was measured using a Si photo-diode, the raw data were obtained in the form of voltage. The photo-diode voltage ratio V/V_0 is plotted on the vertical axis, where V_0 and V are the detected voltage before and after the pump pulse laser irradiation. The V/V_0 starts to relatively sharply decrease at about 26 ns defined as t_{th}, which should mean nucleation time, and then saturate at around 40 ns. Such the decrease in reflectivity should be due to crystallization of the GCT amorphous film.

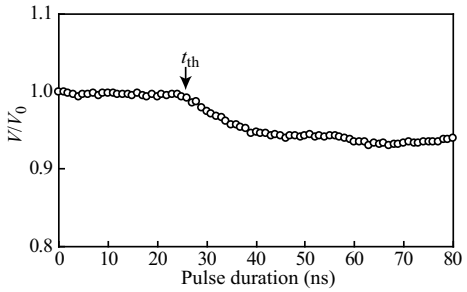

Fig. 5. Reflectance change of the GCT film induced by laser irradiation with a fixed power of 11.0 mW plotted as a function of laser pulse duration.

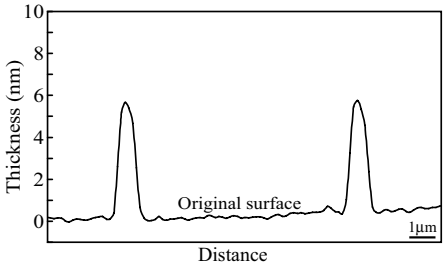

Fig. 6. AFM line profile on the GCT film after the laser irradiation shown in Fig. 5, where the laser irradiation was done twice at different place.

To make sure that the decrease in reflectance is caused by crystallization, the thickness change of the GCT film by laser irradiation was investigated. Very recently, the preset authors have reported that the GCT amorphous film showed the increase in film thickness upon crystallization [2]. Fig. 6 shows the AFM line profile on the GCT film after the laser irradiation shown in Fig. 5, where the laser irradiation was done twice at different place. It is seen that the film thickness increases after the laser irradiation. The thickness increase is estimated to be about 2.7% which is in good agreement with the thickness increase of 2.0% with thermal crystallization [2]. Therefore, the reflectance decrease by the laser irradiation observed in the GCT film is decided to be due to crystallization. Meanwhile, the GST amorphous film showed the reflectance increase after the laser irradiation and the t_{th} of the GST film was estimated to be about 23 ns in the same experimental condition. These results indicate that the nucleation time t_{th} of the GCT amorphous film is only a slightly longer than that of the GST amorphous film. Generally, the nucleation time of amorphous film tends to increase as the crystallization temperature of the amorphous film increases [19]. It is noteworthy that although the GCT amorphous film shows much higher crystallization temperature than the GST amorphous film [2], the nucleation time of the GCT film is nearly equal to that of the GST film. Moreover, Zhou et al. investigated the effects of the recording layer thickness and layer stack structure on the data bit rate of a phase change optical disk made with a Ge-Sb-Te-based recording layer [20]. They showed that the data bit rate increases as the complete crystallization time of the PCM decreases, and that a shorter nucleation time is accompanied by a shorter complete crystallization time. Therefore, the GCT film is expected as a phase change material with both a high crystallization temperature and a not-so-lengthy crystallization time.

3-4. Amorphous structure of GCT

Before simulations of amorphous GCT structure, test runs were carried out to establish minimum interatomic distances. The obtained minimum interatomic distances were 2.35, 3.1, 2.35, 2.45, 2.35, 2.45 Å for Ge-Ge, Ge-Cu, Ge-Te, Cu-Cu, Cu-Te and Te-Te pairs, respectively. Since very good fits could be obtained without Ge-Cu bonding, it seems reasonable to assume that Ge has predominantly Te and Ge neighbors and similarly to other Ge-Te based amorphous. Therefore, each Ge atom was forced to have 4 Ge/Te neighbors. This constraint together with the above minimum interatomic distances was used to obtain the reference configuration.

Table 1. Coordination numbers *Nij* and nearest neighbour distances r_{ij} in amorphous GCT.

	GeGe	GeTe	CuCu	CuTe	TeGe	TeCu	TeTe	Ge total	Cu total	Te total
N_{ij}	1.2	2.8	2.2	2.2	0.93	1.45	1.65	4.0	4.4±0.6	4.0±0.5
r_{ij} [Å]	2.49	2.64	2.58	2.55	2.64	2.55	2.74			

Table 1 shows the simulated results on coordination numbers N_{ij} and nearest neighbor distances r_{ij} in GCT amorphous. It is seen that Te-Te homonuclear bonds are formed in the GCT amorphous and the Te-Te coordination number is 1.65. It has been simulated that in $Ge_2Sb_2Te_5$ amorphous there are no Te-Te bonds and only Ge-Ge homonuclear bonds are formed because the *8-N* rule can not be satisfied without them [4], where *N* is the number of valence electrons formally assigned to the elements. The Te-Te bond length is 2.74 Å, while the Ge-Te bond length is 2.64 Å. Both values agree well with the bond lengths found in glassy $Ge_{20}Te_{80}$ and $Ge_{15}Cu_8Te_{77}$ [5]. The Te-Cu bond length is 2.55 Å which is also in agreement with the values found in Te-rich Ge-Cu-Te glasses [5]. The Cu-Cu coordination number is 2.2, while the Cu-Cu bond length is 2.58 Å. In $Ge_{15}Cu_8Te_{77}$ glass the Cu-Cu coordination number was 1.63, while the Cu-Cu bond length was 2.81 Å. The great difference of the Cu-Cu bond lengths suggests that the interaction between Cu atoms is different in the two compositions. Moreover, Table 1 suggests that the *8-N* rule is not satisfied in the amorphous GCT because the coordination number of Te is around 4 which is much higher than the value of 2 predicted by the *8-N* rule. Further investigations including comparison of GCT amorphous with other amorphous tellurides are under way.

4. CONCLUSION

In this study, we investigated the crystallization mechanism, nucleation time and structure of amorphous GCT prepared by sputter deposition. From a comparison of the crystallization behaviors of the GCT and GST amorphous films it was suggested that the GCT amorphous film shows a growth dominated crystallization process. The

crystalline GCT film showed a lower reflectance than the amorphous GCT film. The nucleation time of the GCT amorphous film was only a slightly longer than that of the GST amorphous film. Therefore, the GCT film is expected as a phase change material with both a high crystallization temperature and a not-so-lengthy crystallization time.

Acknowledgement

This work was supported by the Japan Science and Technology Agency, and KAKENHI (Grant No. 23360297).

REFERENCES

1. Y. Sutou, T. Kamada, M. Sumiya, Y. Saito, J. Koike, Acta Mater. (2012) 872.
2. T. Kamada, Y. Sutou, M. Sumiya, Y. Saito, J. Koike, Thin Solid Films, 520 (2012) 4389.
3. O Gereben, P Jovari, L Temleitner, L Pusztai, J. Optoelectoron Adv. M. (2007) 9, 3021.
4. P. Jóvári, I. Kaban, J. Steiner, B. Beuneu, A. Schops, MA. Webb, Phys. Rev. B (2008) 77, 035202.
5. L. Rátkai, A.P. Gonçalves, G. Delaizir, C. Godart, I. Kaban, B. Beuneu, P. Jóvári, Solid State Communications, (2011) 151, 1524.
6. T. Ozawa, Bull. Chem. Soc. Jpn. (1965) 38, 1881.
7. T. Ozawa, J. Therm. Anal. (1970) 2, 301.
8. W. Lu, B. Yan, W. Huang, J. Non-Cryst. Solids (2005) 351, 3320.
9. JW Christian, The Theory of Transformation in Metals and Alloys, Part I, 2nd Ed. New York: Pergamon Press; 1975.
10. S. Ranganathan, MV. Heimendahl, J. Mater. Sci. (1981) 16, 2401.
11. VRV. Ramanan, GE. Fish, J. Appl. Phys. (1982) 53, 2273.
12. Y. Sutou, T. Kamada, Y. Saito, M. Sumiya, J. Koike, Mater. Res. Soc. Symp. Proc. (2010) 1251, H05-08.
13. KF. Kelton, AL. Greer, CV. Thompson, J. Chem. Phys. (1983) 79, 6261.
14. Qi Chen, L. Liu, KC. Chan, J. Alloy. Comp. (2006) 419, 71.
15. T. Hurst, In: IEEE optical data storage 2000 conference digest; 2000. p. 77.
16. Y. Nishi, H. Kando, M. Terao, Jpn. J. Appl. Phys. (2002) 41, 631.
17. N Yamada, E. Ohno, K. Nishiuchi, N. Akahira, J. Appl. Phys. (1991) 69, 2849.
18. XT. Fu, WD. Song, HW. Ho, R. Ji, L. Wang, MH. Hong, Appl. Phys. Lett. (2012) 100, 201906.
19. L. van Pieterson, MHR. Lankhorst, M. van Schijndel, AET. Kuiper, JHJ. Roosen, J. Appl. Phys. (2005) 97, 083520.
20. GF. Zhou, BAJ. Jacobs, Jpn. J. Appl. Phys. (1999) 38, 1625.

Biographies

Y. Sutou studied materials science at Tohoku University in Japan and received his PhD at the same University in 2001. He is an associate professor of the device reliability science and engineering at Department of Materials Science, Graduate School of Engineering, Tohoku University. His research field is alloy design and microstructural control of shape memory alloys, phase change materials, electrodes for semiconductor, hard coating etc.